frontiers | Frontiers in Marine Science

TYPE Original Research
PUBLISHED 13 September 2024
DOI 10.3389/fmars.2024.1427524

OPEN ACCESS

EDITED BY
Jun Sun,
China University of Geosciences (Wuhan), China

REVIEWED BY
Stella Psarra,
Hellenic Centre for Marine Research (HCMR), Greece
Yuqiu Wei,
Chinese Academy of Fishery Sciences (CAFS), China
Meilin Wu,
Chinese Academy of Sciences (CAS), China

*CORRESPONDENCE
Benjamin A. S. Van Mooy
bvanmooy@whoi.edu

RECEIVED 03 May 2024
ACCEPTED 20 August 2024
PUBLISHED 13 September 2024

CITATION
Bent SM, Muratore D, Becker KW, Barone B, Clemente T, Fredricks HF, Holm HC, Karl DM and Van Mooy BAS (2024) Lipid biochemical diversity and dynamics reveal phytoplankton nutrient-stress responses and carbon export mechanisms in mesoscale eddies in the North Pacific Subtropical Gyre.
Front. Mar. Sci. 11:1427524.
doi: 10.3389/fmars.2024.1427524

Lipid biochemical diversity and dynamics reveal phytoplankton nutrient-stress responses and carbon export mechanisms in mesoscale eddies in the North Pacific Subtropical Gyre

Shavonna M. Bent[1,2], Daniel Muratore[3], Kevin W. Becker[1,4], Benedetto Barone[5], Tara Clemente[5], Helen F. Fredricks[1], Henry C. Holm[1,2], David M. Karl[5] and Benjamin A. S. Van Mooy[1]*

[1]Department of Marine Chemistry & Geochemistry, Woods Hole Oceanographic Institution (WHOI), Woods Hole, MA, United States, [2]Department of Earth, Atmospheric & Planetary Sciences, Massachussetts Institute of Technology (MIT), MIT – WHOI Joint Program in Oceanography/Applied Ocean Science & Engineering, Cambridge, MA, United States, [3]Santa Fe Institute, Santa Fe, NM, United States, [4]GEOMAR Helmholtz Centre for Ocean Research Kiel, Kiel, Germany, [5]Daniel K. Inouye Center for Microbial Oceanography: Research and Education, University of Hawai'i at Mānoa, Honolulu, HI, United States

Mesoscale eddies cause deviations from the background physical and biogeochemical states of the oligotrophic oceans, but how these perturbations manifest in microbial ecosystem functioning, such as community macromolecular composition or carbon export, remains poorly characterized. We present comparative lipidomes from communities entrained in two eddies of opposite polarities (cyclone–anticyclone) in the North Pacific Subtropical Gyre (NPSG). A previous work on this two-eddy system has shown differences in particulate inorganic carbon (PIC) and biogenic silica sinking fluxes between the two eddies despite comparable total organic carbon fluxes. We measured the striking differences between the lipidomes of suspended and sinking particles that indicate taxon-specific responses to mesoscale perturbations. Specifically, cyanobacteria did not appear to respond to increased concentrations of phosphorus in the subsurface of the cyclonic eddy, while eukaryotic microbes exhibit P-stress relief as reflected in their lipid signatures. Furthermore, we found that two classes of lipids drive differences between suspended and sinking material: sinking particles are comparatively enriched in phosphatidylcholine (PC, a membrane-associated lipid) and triacylglycerol (TAG, an energy storage lipid). We observed significantly greater export of TAGs from the cyclonic eddy as compared to the anticyclone and found that this flux is strongly correlated with the

concentration of ballast minerals (PIC and biogenic silica). This increased export of TAGs from the cyclone, but not the anticyclone, suggests that cyclonic eddy perturbations may be a mechanism for the delivery of energy-rich organic material below the euphotic zone.

KEYWORDS

lipids, surface ocean biogeochemistry, mesoscale eddies, nutrient stress, ballast minerals

Introduction

Mesoscale eddies are prevalent throughout the world's oceans (Chelton et al., 2011) and alter the biogeochemical state of the water column during their passage (Sweeney et al., 2003). Cyclonic eddies are associated with isopycnal uplifting that can result in the delivery of nutrients to the upper euphotic zone. Anticyclonic eddies are associated with a depression of isopycnals that moves nutrient-rich waters below the euphotic zone (McGillicuddy, 2016; Barone et al., 2019). While some studies have shown that upwelling during eddy intensification can increase primary production (Falkowski et al., 1991; Seki et al., 2001; Singh et al., 2015), others in the North Pacific Subtropical Gyre (NPSG) found no change in primary production despite increases in nutrient concentration in the lower euphotic zone (Barone et al., 2019). However, even if primary production does not consistently increase in cyclonic eddies, the isopycnal uplift results in steeper nutrient gradients and increased abundance of eukaryotic phytoplankton in the subsurface ocean (Barone et al., 2022).

Regardless of conflicting evidence on the impact of cyclonic eddies on primary production, both cyclonic and anticyclonic eddies represent significant deviations from the background biogeochemistry within the NPSG at Station ALOHA (A Long-term Oligotrophic Habitat Assessment). Both eddy types alter particulate and dissolved stocks of inorganic and organic nutrients (Barone et al., 2019, 2022). A pair of adjacent eddies of opposite polarity sampled in 2017 showed a significant relationship between corrected sea-level anomaly (abbr. SLA, inversely proportional to the vertical displacement of water layers in the ocean interior) and the export flux of sinking particulate matter from the euphotic zone (Barone et al., 2022). This finding highlights that eddies can result in significant deviations from average export rates, suggesting a need to identify ecological or physiological mechanisms underlying export beyond increased total primary production.

Barone et al. (2022) hypothesized that changes in phytoplankton community structure led to differences in export between eddies. Lipid compositions and concentrations are powerful indicators of both community structure (Popendorf et al., 2011) and physiological stressors, such as temperature (Hixson and Arts, 2016; Holm et al., 2022), light (Wacker et al., 2016; Becker et al., 2018; Muratore et al., 2022), and nutrient scarcity (Van Mooy et al., 2006, 2009). Several reviews have detailed the use of lipidomics in studying a variety of environmental changes and variability, as well as impacts on human health and biogeochemical cycling (Parrish, 2013; Koelmel et al., 2020). Because lipids are impacted not only by community structure but also by several abiotic and biotic factors, the systematic analysis of lipid biochemical diversity and dynamics provides a powerful tool for studying ecological and physiological responses of phytoplankton to environmental perturbations. These responses include changes in nutrients and light induced by isopycnal displacement from eddies. Therefore, we used comparative lipidomics to identify shifts in community composition and functional response to the two eddies surveyed by this expedition.

We compared potential nutrient-stress responses using established and emerging lipidomic nutrient-stress indicators in two mesoscale eddies previously described by Barone et al. (2022). Within two major depth layers analyzed in each of the two eddies [i.e., surface and deep chlorophyll maximum (DCM) within cyclone and anticyclone], there are distinct changes in community lipidomes that are not entirely dependent on community composition. We further examine how these changes manifest in POM exported from the euphotic zone collected from sediment traps. While the total particulate organic carbon (POC) flux was not significantly different between eddies (Barone et al., 2022), we observed increased export of triacylglycerols (TAGs), an energy storage lipid, in the cyclonic eddy. This increase in TAGs is correlated to increased total mass export and ballast mineral export in the cyclone (Barone et al., 2022). Thus, through the lens of lipidomics, we find evidence for the biological pump to become more efficient at exporting energy-rich, labile POM under cyclonic mesoscale perturbances, despite similar total fluxes of organic carbon from other areas of the water column.

Materials and methods

Cruise setting and field collection

The Microbial Ecology of the Surface Ocean – Simons Collaboration on Ocean Processes and Ecology (MESO-SCOPE) cruise in late June to early July of 2017 (KM1709) sampled across two adjacent eddies of opposite polarities, located near Station

ALOHA in the NPSG. Eddies were identified using satellite measurements of SLA (Barone et al., 2022), which was corrected to remove the interannual trend and the seasonal cycle, according to the methods of Barone et al. (2019). Samples were collected along a transect across the eddies, as well as in a Lagrangian fashion over the course of 3 days within each eddy center, during which the ship followed a Surface Velocity Program drifter (Pacific Gyre Inc., Oceanside, CA), with a drogue centered at 15 meters (m) depth. Water from 15 m, 75 m, 100 m, the DCM (ranging from 103 to 130 m), 125 m, and 175 m was collected for lipidomic analysis using a Niskin® bottle rosette. One to 2 L of seawater from each depth was vacuum-filtered onto 47-mm diameter 0.22-µm hydrophilic Durapore filters (MilliporeSigma, Burlington, MA). Filters were flash frozen in liquid nitrogen and stored in liquid nitrogen at −196° C until processed.

Particle interceptor traps (PITs) (Knauer et al., 1979; Grabowski et al., 2019; Karl et al., 2021) were used to obtain sinking particle samples for lipidomic analysis. Before deployment, PIT tubes (0.0039 m^2 collection area) were filled with 0.4 L of formaldehyde-poisoned salt brine (1.05 g/cc density) prepared from 0.2 µm of filtered surface seawater. Free drifting surface-tethered PITs were deployed across the eddy field (Figure 1A, open circles) with a single 12-tube array for particle collection at 150 m depth for 9 to 12 days. Bulk fluxes of particulate organic carbon (POC), inorganic carbon (PIC), phosphorus (PP), nitrogen (PN), biogenic silica (PSi), and total mass were collected alongside samples for lipidomic analysis. Materials and methods for the determination of these fluxes, as well as data for these bulk fluxes, can be found in Barone et al. (2022). Importantly, a 335-µm mesh was used to remove zooplankton before sample processing. Notably, sinking POM for lipidomic analysis was processed by filtering onto triplicate GF/A filters (nominal porosity 1.6 µm, exceptions for traps 7, 8, and 11, n = 2, and trap 6, n = 4), rather than GF/F filters (used for bulk fluxes of POC, etc.), to prevent the material from clogging the filter. Filters were stored in liquid nitrogen at −196°C until sample processing. The average for each trap was used for analysis, after normalization to length of deployment (Supplementary Table 1) and trap area.

Lipid sample processing

Total lipid extracts (TLEs) were obtained from all samples using a modified Bligh & Dyer extraction (Bligh and Dyer, 1959), previously described by Popendorf et al. (2013) and more recently by Holm et al. (2022). Briefly, sample filters were added to a mixture of dichloromethane (1.0 mL, GC Resolv grade, Thermo Fisher, Waltham MA), methanol (2.0 mL, GC Resolv grade, Thermo Fisher), and phosphate-buffered saline (0.8 mL, Thermo Fisher PBS, standard recipe, pH = 7.4, 137 mM of NaCl, 2.7 mM of KCl, 10 mM of Na_2HPO_4, and 1.8 mM of KH_2PO_4) and vortexed to mix well. An injection of 20 µL of 0.05 mg mL^{-1} 2,4-dinitrophenyl phosphatidylethanolamine diacylglycerol (DNP-PE, Avanti Polar Lipids Inc, Alabaster, AL) dissolved in dichloromethane was added, and samples were vortexed again and then sonicated for 10 min. Another 1.0 mL from each of phosphate-buffered saline and dichloromethane was added to complete the extraction of lipids into the organic phase. Vials were centrifuged at 400g to speed the

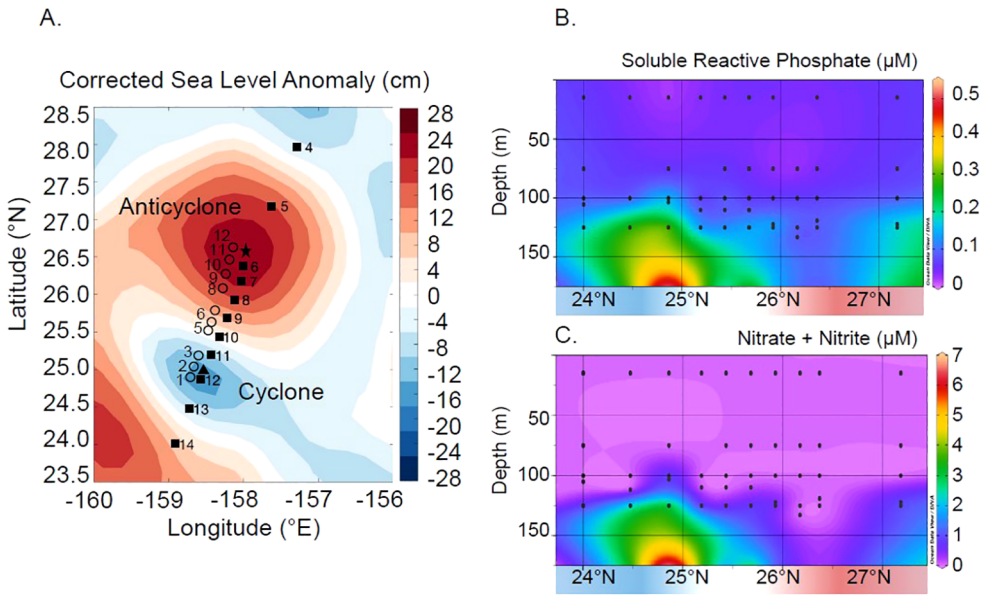

FIGURE 1
Sample location map **(A)** superimposed into a map of corrected sea-level anomaly (SLA) during the time of sampling. The water column (closed square), sediment trap (open circle), and Lagrangian (closed triangle and star) sampling sites are shown. Sediment traps were deployed at the location depicted and drifted for 9 to 12 days before recovery. Lagrangian samples were collected from each eddy center over the course of ~3 days at water column station 12 (cyclone, closed triangle) and station 6 (anticyclone, closed star). Also shown is the impact of eddies along the transect on concentrations of soluble reactive phosphorus (SRP, µM P) **(B)** and dissolved inorganic nitrogen (either nitrate + nitrite measurements or low-level nitrate measurements, depending on background concentrations and assay sensitivity; µM N) **(C)**.

separation of the organic and polar phases. The bottom organic phase, or TLE, of the mixture was removed, 10 µL of 1.5 mM butylated hydroxytoluene was added to prevent sample oxidation, and the TLE was stored under argon gas at −20°C until mass spectral analysis.

Samples were processed using high-performance liquid chromatography (HPLC) and high-resolution accurate-mass mass spectrometry (HRAM-MS), with a Q-Exactive Orbitrap (Thermo Fisher) and electrospray ionization analysis. To optimize samples for HPLC analysis, a 50-µL aliquot of the TLE was dried down under N_2 gas and redissolved with 50 µL of acetonitrile and isopropyl alcohol (ACN: IPA, 70:30 ratio). See Supplementary Table 2 for further details on the HPLC/HRAM-MS instrument conditions. Spectra were collected over the course of the run in alternating positive and negative ionization modes. External standard curves were run alongside the samples to allow for subsequent quantification (Supplementary Table 3).

Lipidomic annotation and identification

The R language package and pipeline, *LOBSTAHS* (Collins et al., 2016), was used to identify lipid features from raw spectral data. Mass features were first detected and grouped across samples, and retention time was aligned using the R package *xcms* (Smith et al., 2006). Missing values from peak groups across samples were reintegrated to quantify peaks possibly missed by initial peak detection (i.e., peak filling). Features were then grouped into "pseudospectra" (i.e., groups of peak-groups), using the *CAMERA* package (Kuhl et al., 2012). Pseudospectra include all peak-groups of adducts and isotope features likely derived from the same compound. Data were then imported into *LOBSTAHS* for screening against an *in-silico* database and final annotation as possible lipid compounds. The raw output of the *LOBSTAHS* pipeline is putative peak annotations based on comparison with previously positively identified lipid compounds. See Supplementary Table 4 for complete parameters and methods used in mass spectral processing.

We validated annotations of possible lipid species using the following parameters: accurate mass, adduct hierarchies, retention time patterning, and MS^2 fragmentation spectra (Collins et al., 2016; Becker et al., 2018; Holm et al., 2022). In total, we retained 659 lipid features from the total annotated output, 161 of which were manually confirmed by checking positive and negative modes for the correct adduct formation or the presence of MS^2. These high-confidence lipids were used to build the patterning upon which the other lipids were confirmed. Lipid peak areas were quantified to picograms on column using a suite of external standard curves. The external standard used for each lipid class is listed in Supplementary Table 3 and is based on the work conducted by Popendorf et al. (2013). Finally, we accounted for recovery efficiency during the extraction process by normalizing to the amount of internal standard (DNP-PE) that was spiked in versus the amount that was observed in each sample. The quantitative rigor of this external standard approach, particularly for the quantification of TAGs, has been previously described (Becker et al., 2018). The quantification of TAGs, which is especially relevant to C:P calculations, relies specifically on the equivalent carbon number approach described by Becker et al. (2018) and the predictable behavior these molecules exhibit when accounting for acyl chain length and number of double bonds.

Visualization and statistical analysis

The software Ocean Data View (Schlitzer, 2022) was used for data visualization across the eddy transect. RStudio (R Core Team, 2023) was used for all other statistical analysis; the packages used and their primary purposes are listed in Supplementary Table 4. Throughout the manuscript, a p-value of <0.05 was used to determine a significant result. Redundancy analysis (RDA) was performed using the *vegan* package (Oksanen et al., 2020), first log-normalizing lipid concentrations of both suspended and sinking samples to account for heteroskedasticity. We used the following metadata as environmental covariates for the water column RDA: corrected SLA, depth, and cell counts for picoeukaryotes, heterotrophic bacteria, and *Prochlorococcus* [for the collection methods, see Barone et al. (2022)]. Additionally, we tested the potential for autocorrelation due to Lagrangian sampling to drive the observed relationships by including sample day and time in the covariate matrix. Environmental covariates for the RDA of sediment trap data included the fluxes of particulate phosphorus, nitrogen, biogenic silica, and mass, as well as the particulate inorganic and organic carbon fluxes (Barone et al., 2022). Soluble reactive phosphorus (SRP) was used to determine bioavailable inorganic P concentrations, while low-level nitrogen (LLN) and nitrate + nitrite (N+N) measurements were combined to obtain the best coverage for inorganic nitrogen availability across the transect, dependent on background concentrations and detection limits for each assay. Methods for the determination of nutrient concentrations followed the standard protocols for Station ALOHA and can be accessed at https://hahana.soest.hawaii.edu/hot/methods/llnuts.html. Briefly, SRP concentrations were determined following Karl and Tien (1992), while the methods for dissolved nitrogen concentrations followed the work of Foreman et al. (2016).

To examine signs of nutrient stress across the study transect, we utilized a previous work which established that in response to phosphorus stress (P-stress), cyanobacteria substitute phospholipids, primarily phosphatidylglycerol (PG), for the structurally similar sulfoquinovosyldiacylglycerol (SQDG) (Van Mooy et al., 2006, 2009). The ratio of these two lipids, SQDG: PG, can be used as a marker for P-stress in the environment. Similarly, in response to P-stress, eukaryotic phytoplankton substitute their primary phospholipid, phosphatidylcholine (PC), for one of three betaine lipids (BLs): diacylglyceryl trimethylhomoserine, DGTS; diacylglyceryl hydroxymethyl-trimethyl-β-alanine, DGTA; or diacylglyceryl carboxyhydroxymethlycholine, DGCC (Van Mooy et al., 2009). This stress response is reported as the ratio of betaine lipids to phosphatidylcholine: the BL: PC ratio. In addition to betaine lipid substitution, eukaryotic algae have previously been shown to upregulate the production of TAGs under nutrient-stress conditions, particularly N-starvation (Goncalves et al., 2016). The SQDG: PG and

BL: PC stress signals are ratios that rely on the substitution of structurally similar lipids for one another; SQDG and PG are both anionic, while the three betaine lipids and PC are all zwitterionic, within the pH range of seawater; the use of lipid ratios helps to reduce noise in the signal from variations in the concentration of biomass. We compare the concentration of TAGs (Figure 2H) to total picoeukaryote counts across the transect (Figure 2I), resulting in the TAG: Picoeukaryote ratio (TAG: Picoeuk ratio, Figure 2G), which allows us to better assess the levels of stress per cell, rather than tracking biomass. Other lipid groups of interest included monogalactosyldiacylglycerol (MGDG), digalactosyldiacylglycerol (DGDG), and phosphatidylethanolamine (PE).

The daily steady-state lipid export rate, with units of day^{-1}, is defined as the quotient of the export flux at 150 m and water column inventory from 0 m to 150 m at each eddy center. The lipid inventory was calculated via the "spline" method from the R package DescTools (Signorell, 2021), which integrates the water column profile for each lipid. The export flux at 150 m was calculated using the average of two PIT arrays in the cyclonic eddy center (traps 1 and 2) and an average of three PIT arrays in the anticyclonic eddy center (traps 10, 11, and 12). We used the lipid flux from these same traps to calculate the relative abundance of lipid classes in exported POM from each eddy. We also calculated the relative abundance of lipids within the water column data from station 12 (cyclonic eddy center) and station 6 (anticyclonic eddy center). The C:P ratio of the lipidome was calculated by converting from μg L^{-1} to mol L^{-1} using the molecular formula and weight of each lipid to obtain moles of carbon and phosphorus. The total amount of each element was summed and the C:P ratio was calculated using those totals. TAGs, which show differential export between the two eddies, are carbon-rich but do not contain any phosphorus or nitrogen. Thus, to determine their impact on export biogeochemistry, we calculated the C:P ratio with and without these molecules included. We selected the C:P

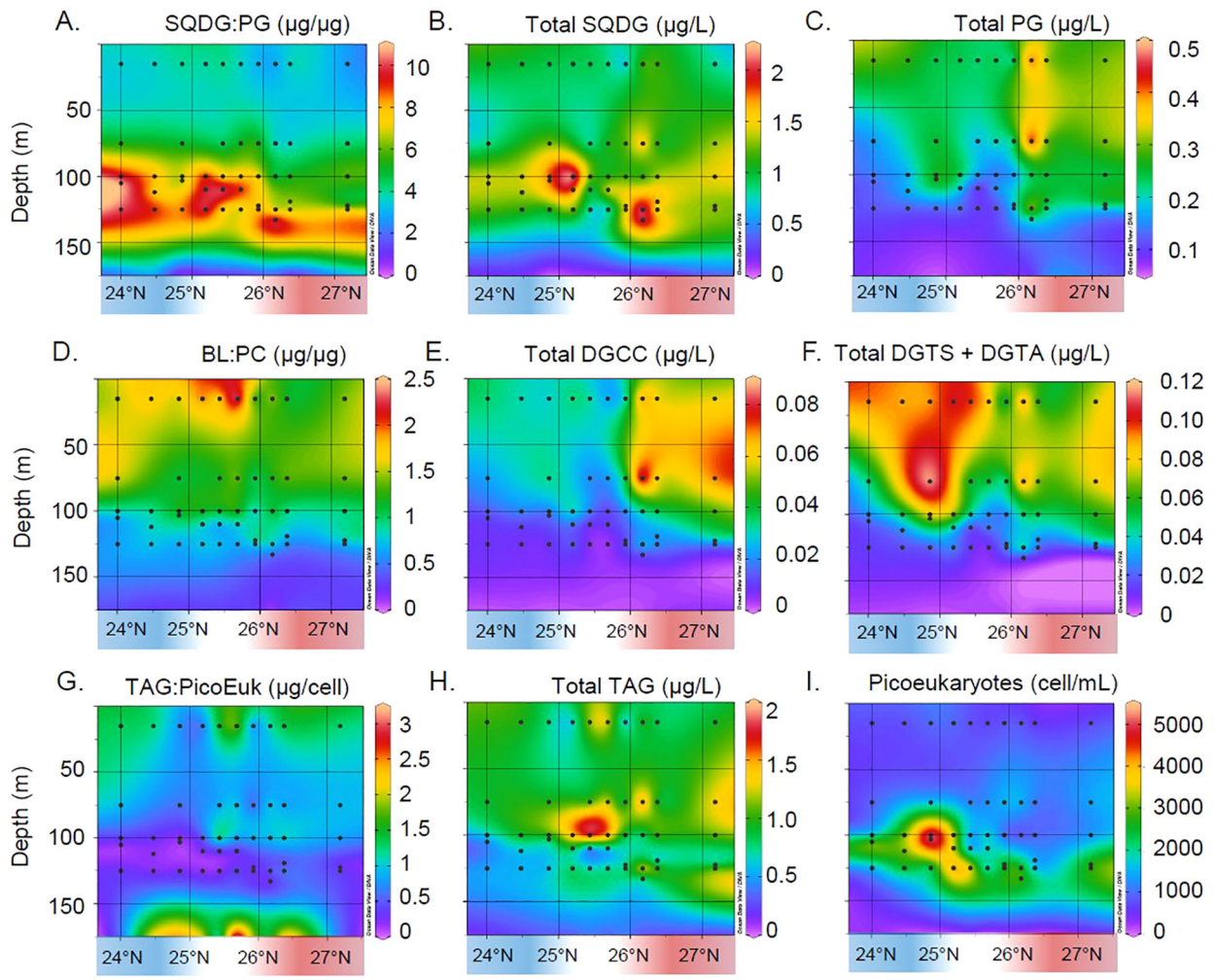

FIGURE 2
Canonical signals of stress within the lipidome of the water column across the eddy transect are shown in the top two sets of plots; the prokaryotic lipidomic signal and associated molecules are shown in **(A–C)**; the eukaryotic lipidome and constituent betaine lipids (BLs) are given in **(D–F)**. Less well studied but increasingly recognized is the production of TAGs in response to nutrient stress; a normalized TAG: Picoeuk count is shown in **(G)**, with concentrations of TAG given in **(H)** and count data presented in **(I)**.

ratio rather than the C:N ratio as eukaryotic signs of nutrient stress appeared to be responding to differential patterns of P, rather than N, across the transect.

Results

Biogeochemical conditions vary across eddy polarities

We collected 10 depth profiles of suspended lipids from 15 m to 175 m across the MESO-SCOPE eddy transect (Figure 1A). Lipidome samples were paired with measurements of the macronutrients phosphorus (SRP) and nitrogen (N+N) (Figures 1B, C). SRP concentrations in the upper 175 m varied from a minimum of 0.023 μmol L^{-1} on the surface of the cyclonic eddy to a maximum of 0.513 μmol L^{-1} P at 175 m within the cyclonic eddy. N+N concentrations followed a similar pattern, varying between levels below detection limits (N < 2 nM) to a maximum of 6.634 μmol L^{-1} N at the base of the cyclonic eddy. N:P values of dissolved inorganic nutrients (i.e., N+N and SRP) remain below 10 across the transect within the surface (i.e., above 100 m).

Nutrient-stress responses are stronger in eukaryotic lipid biomarkers than cyanobacteria between eddies

Cyanobacteria substitute phospholipid PG for a non-phosphorus lipid, SQDG, in response to phosphorus stress (P-stress) (Van Mooy et al., 2006, 2009). Across both eddies, the SQDG: PG ratio was the highest at the DCM (mean ± standard deviation within DCM samples of 8.2 ± 1.6), with the highest values observed in the DCM of the cyclonic eddy (Figure 2A). This pattern appears to be driven both by the higher concentrations of SQDG at the DCM across the transect (Figure 2B) and changes in the concentrations of PG (Figure 2C). SQDG concentrations reach a maximum of 2.2 μg L^{-1} across the DCM of the transect, while PG is consistently <0.3 μg L^{-1} in this same area. Because SQDG is associated with the thylakoid membrane, its variability can be driven by photoadaptation, particularly by *Prochlorococcus* which uses divinyl chlorophyll *a* (Supplementary Figure 1A). To determine the relative importance of P-stress and photoadaptation on the SQDG: PG ratio, we compared it with SRP (Supplementary Figure 1B) and divinyl chlorophyll *a* concentrations (Supplementary Figure 1C). SRP is not significantly correlated with SQDG: PG (Spearman's rank correlation, rho = 0.07, p = 0.57), while the correlation with divinyl chlorophyll *a* is significant (Spearman's rho = 0.80, p < 0.001). Thus, during the MESO-SCOPE cruise, we find that SQDG replacement of PG is more strongly associated with cyanobacterial photoadaptation than local SRP concentrations.

Eukaryotic phytoplankton have been shown to substitute their primary phospholipid (PC) for BLs in response to P-stress (Van Mooy et al., 2009). We measured the lowest values of BL: PC across the DCM of the transect (Figure 2D; Supplementary Figure 8) and the highest BL: PC values near the surface of the cyclonic eddy, where SRP concentrations were the lowest (Figure 1B). The BL: PC ratio varies from 0.1 to 2.4 across the transect, with minima at the DCM (0.74 ± 0.14). Unlike the SQDG: PG ratio, the betaine lipids in the numerator are the sum of three distinct lipid classes, DGCC, DGTA, and DGTS; the latter two are not distinguished from one another with our HPLC/HRAM-MS method. Concentrations of DGCC are elevated on the surface of the anticyclone (Figure 2E), reaching a maximum of 0.086 μg L^{-1}. Concentrations of the betaine lipid classes DGTS+DGTA are elevated primarily on the surface of the cyclonic eddy (Figure 2F), peaking at concentrations of 0.117 μg L^{-1}. PC concentrations have a more homogeneous distribution across eddies (Supplementary Figure 2A), with a peak above the DCM of the cyclonic eddy. There is a significant correlation between BL: PC and SRP (Supplementary Figure 2B, Spearman's rho = −0.79, p < 0.001). Thus, eukaryotic phytoplankton generally follow expected patterns of P-stress response: P-stress is the least across the DCM of the transect, where SRP is enhanced, and the highest near the surface of the cyclone where SRP reaches minimum concentrations.

Recent work has shown that eukaryotic phytoplankton produce greater amounts of TAGs in response to nutrient stress (Merchant et al., 2012; Goncalves et al., 2016). We therefore used flow cytometric picoeukaryotic phytoplankton cell counts (see *Methods*) to calculate a TAG: Picoeuk ratio for each sample to identify relative TAG overproduction as a putative nutrient-stress biomarker. We found the lowest TAG: Picoeuk in the DCM of the cyclonic eddy and a range from 0.14 to 3.1 across the transect. Low values of the TAG: Picoeuk ratio in the DCM of the cyclonic eddy are consistent with the alleviation of P-stress suggested by the BL: PC ratio. The TAG: Picoeuk ratio is significantly correlated with SRP concentrations (Spearman's rho = −0.27, p = 0.05, Supplementary Figure 3A), but not with nitrogen concentrations (Spearman's rho = −0.19, p = 0.15).

Beyond specific biomarkers of nutrient stress, we also studied the differences in the overall lipid makeup of phytoplankton communities in each eddy. We identified 454 individual lipid compounds within 10 classes. These 454 lipids, along with the summed class totals across each sample, were used to perform RDA on the water column lipidome (Figure 3). We tested the potential for autocorrelation within the Lagrangian sampling scheme to drive the observed relationships and found that sample order was not correlated to RDA coordinates [analysis of variance (ANOVA) p > 0.05]. The RDA of water column samples yielded four distinct, significantly different, clusters based on the eddy status and depth (ANOVA, p = 0.005). Samples within the anticyclonic eddy along RDA axis 2 have greater spread within RDA space than that of the cyclonic eddy, potentially suggesting more lipidome variation within the anticyclone as compared to the cyclone (Figure 3). RDA axis 1 accounts for 31.7% of the variance observed within the lipidome, and the separation along this axis is primarily correlated to depth, seen by the clear distinction between the surface and DCM, regardless of eddy polarity (ANOVA, depth, p = 0.001). The difference between eddies is correlated to RDA axis 2 which accounts for 9.8% of the variance within the lipidome. Sea-level anomaly, a proxy for eddy position, was significant within the

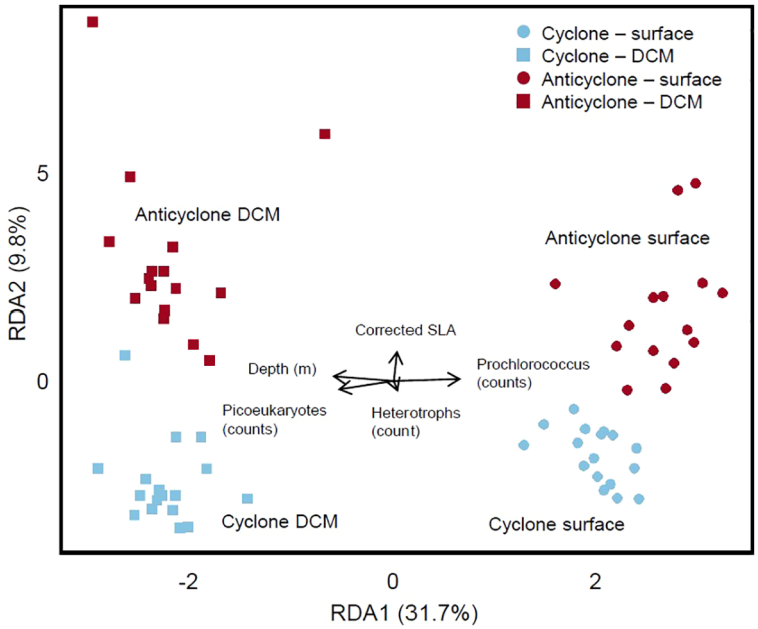

FIGURE 3
Redundancy analysis (RDA) of water column lipidomes sampled from Lagrangian stations (Figure 1A) within the eddy centers over the course of 3 days. Lipid sample compositions are primarily influenced by depth (RDA1), as seen in the consistent separation between surface and DCM lipidomes. Further separation occurs by the eddy sampled (RDA2), seen in the separation of cyclonic and anticyclonic lipidomes, regardless of sampling depth.

model (ANOVA, $p = 0.001$). The RDA model associates *Prochlorococcus* counts with the surface samples and picoeukaryote counts with the DCM samples, in line with observed results from flow cytometry and the imaging flow cytobot, presented in Barone et al. (2022). Briefly, in each eddy center, counts for *Procholorococcus* cells were elevated at the surface as compared to the DCM (average 192,100 ± 19,300 counts at the surface and 68,400 ± 15,300 counts at the DCM). The pattern was reversed for picoeukaryotes, which averaged 3,200 ± 1,000 counts at the DCM and 700 ± 200 counts at the surface. Both *Prochlorococcus* and picoeukaryote counts contribute significantly to the observed differences within the model (ANOVA, $p = 0.004$, $p = 0.009$), while heterotrophic bacterial counts do not (ANOVA, $p = 0.21$).

Sinking particulate matter in cyclonic eddies is enriched in energy storage lipids relative to anticyclone

The relative abundance of each lipid class was calculated within the water column and exported POM captured in sediment traps for each eddy center (Figure 4). In the water column, thylakoid-associated lipids (SQDG, MGDG, and DGDG) are the predominant constituents of the suspended lipidomes. The relative abundance of this group of molecules decreases from a maximum of 64.3% ± 4.3% in the DCM (103 m to 130 m) of each eddy, to less than 1% within the sediment trap samples. Betaine lipids comprise a relatively small proportion of total lipids within the water column, averaging 0.71% ± 0.45% for DGCC and 1.37% ± 0.9% for DGTS+DGTA (Figure 4). The proportion of betaine lipids within sediment trap samples is even lower, averaging less than 0.1% in each trap, regardless of the lipid class. TAGs are the most abundant lipids in sinking particles, making up 82% and 70% of the lipid content for the cyclone and anticyclone, respectively. In contrast, TAGs make up 26.7% ± 12% of lipid content in suspended particles (Figure 4). PC is the second most abundant lipid within sinking POM, comprising 15% and 24.6% of cyclone and anticyclone sediment trap lipidomes, respectively. Additionally, PC comprises nearly all of the phospholipid content within sinking POM: the other phospholipids (PG and PE) make up less than 5% of sinking lipids. In contrast, PC comprises only 2.3% ± 0.6% of suspended particulate lipidomes, while PE accounts for 8.0% ± 3.9% of water column lipidomes, with PG accounting for 7.7% ± 3.5%. These findings highlight the importance of TAGs and PC within exported particulate matter, despite their relatively smaller contribution to the lipidomes of the water column.

For each lipid class involved in calculating a stress response (SQDG, PG, betaine lipids, PC), the daily lipid export rate was calculated (Figure 5, see *Methods*). All cyanobacterial-associated lipids had low rates of export (<1% day^{-1}). The export rate of divinyl chlorophyll *a* exhibited the lowest rate values, followed by SQDG and PG. The betaine lipids, which are associated with the eukaryotic BL: PC stress response signal, also had an export rate <1% day^{-1}. Betaine lipid export rates were higher than cyanobacteria-associated lipid export rates, but lower than export rates of other eukaryote-associated lipids (PCs and TAGs). Both PC and TAGs exhibited high rates of export, with 19.1% to 32.9% and 4.7% to 20.6% exported each day from the anticyclone and cyclone, respectively. Both betaine lipids and lipids from cyanobacteria were exported slowly, regardless of eddy status. PC, associated with

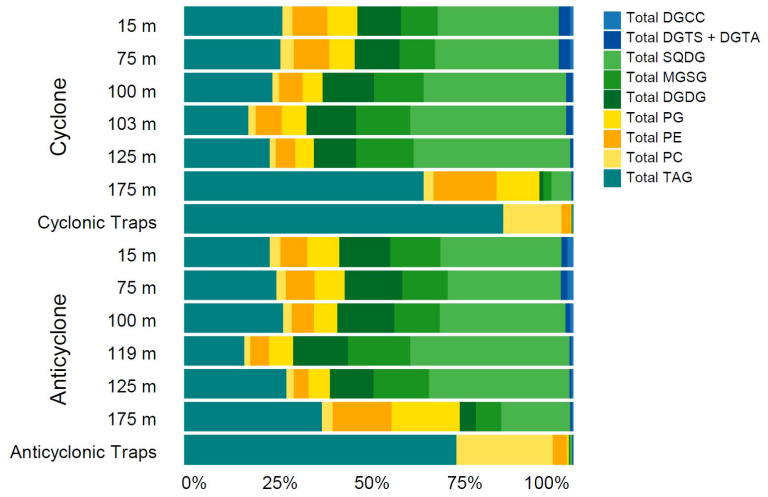

FIGURE 4
Relative abundance of lipid classes within the center of each eddy, as well as the average relative abundance from the export flux collected from the traps deployed in each eddy center (cyclonic traps 1 and 2; anticyclonic traps 10, 11, and 12).

increased concentrations of phosphorus, and TAGs, which were associated with P-stress but are energy storage molecules, were exported rapidly from the euphotic zone. There was also a significantly greater total export of TAGs from the cyclonic eddy center as compared to the anticyclone (Supplementary Figure 4, Welch's *t*-test, $p = 0.036$). While other lipid classes appeared to follow similar trends (i.e., PC), these differences were not significant (PC, $p = 0.074$; Supplementary Table 5).

To determine the lipids driving changes in exported particulate matter, we performed redundancy analysis on the sediment trap samples. In total, 580 individual lipid species were identified from the traps from across 10 lipid classes. The RDA of these lipids and their class totals showed that 38.3% of the variance in the lipidome could be explained along RDA axis 1 (Figure 6). The separation of samples along this axis is primarily by deployment location, with traps along the eddy front (#6 and #8) located between the two clusters from the centers. For the sediment trap RDA, flux measurements were used as the environmental covariate matrix. We observed greater loading of biogenic silica flux (PSi), particulate inorganic carbon (PIC), and mass with the cyclone in RDA space although these relationships are not significant (ANOVA, $p > 0.05$). However, we found that differences in TAG export between eddies were identified as an important driver of sediment trap lipidome composition. TAG export was strongly and positively correlated with the export of both ballast minerals (PSi and PIC, Supplementary Figures 5, 6).

Finding that lipids extracted from sediment traps strongly differed between eddies and that sinking lipids were systematically

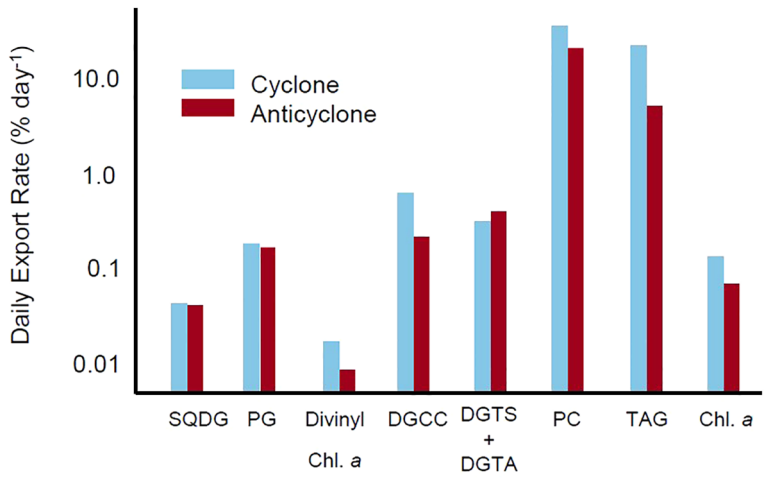

FIGURE 5
The daily lipid turnover rate (percent day^{-1}) calculated by taking the quotient of the export flux and the inventory of each lipid class within the eddy center (stations 6 and 12, see Figure 1A). Results are shown for selected lipid classes, including those associated with prokaryotic stress (SQDG and PG) and eukaryotic stress (PC, DGCC, DGTS+DGTA, and TAG). Divinyl chlorophyll *a* and chlorophyll *a* export rate constants are provided for context.

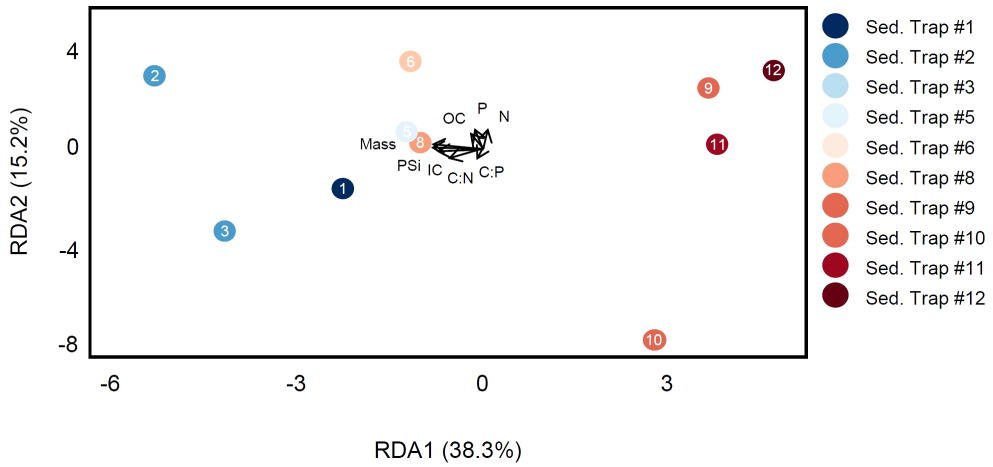

FIGURE 6
RDA of sediment trap lipidomes shows separation by eddy status along RDA1. Environmental flux data (units of mg m^{-2} day^{-1}) were used as the explanatory covariate data matrix and included the flux of overall mass, biogenic silica (PSi), inorganic carbon (IC), organic carbon (OC), nitrogen (N), and phosphorus (P) although these factors were not significantly correlated in RDA space.

different from suspended lipids, we then asked to what extent the difference in lipid composition affected the C:P molar ratio of lipid export. C:P ratios of water column lipidomes had a mean of 186.6 ± 53.4 with a range of 70–340 (Supplementary Figure 7). Lipid C:P ratios from sediment traps were generally higher, with a mean of 234 ± 81.6 and a range of 127–370 (Figure 7). We also found that C:P values of sediment trap lipids were significantly higher from traps deployed in the cyclonic eddy as opposed to the anticyclone (rho between C:P and corrected SLA = −0.76, $p = 0.02$). TAGs, which do not contain P, are a greater fraction of lipid export in the cyclone than the anticyclone and, thus, contribute significantly to the observed differences in the C:P of lipid export. While total POC export is similar between eddies (Barone et al., 2022), exported lipids in cyclonic eddies are more carbon-rich on average.

Discussion

Community lipidomes elucidate patterns in microbial structure and nutrient-stress response

Lipidomic composition delineates microbial communities across eddies and depth layers by taxonomic composition and reveals underlying differences in physiological adaptations for these organisms to local nutrient and light availability. Environmental observations collected during the cruise and published elsewhere (Barone et al., 2022) demonstrated the clear impact that changes in SLA had on ocean biogeochemistry during the passage of these eddies. We find differences in nutrient-stress response lipids among eukaryotic phytoplankton within the water column, but not in the cyanobacterial community. Cyanobacteria, which are highly adapted to the oligotrophic waters at Station ALOHA, did not significantly shift their lipid pools in response to increased concentrations of phosphorus, as indicated by the lack of correlation between SQDG: PG and SRP. Indeed, the much stronger relationship between SDQG and divinyl chlorophyll *a* indicates that light attenuation and photoadaptation was likely the dominant control on the amount of SQDG in this study. As cyanobacteria are adapted to low P concentrations (Bertilsson et al., 2003; Klausmeier et al., 2004), this finding is not surprising. In contrast, the eukaryotic phytoplankton exhibited a response in line with our hypotheses: the strong correlation between BL: PC and SRP shows

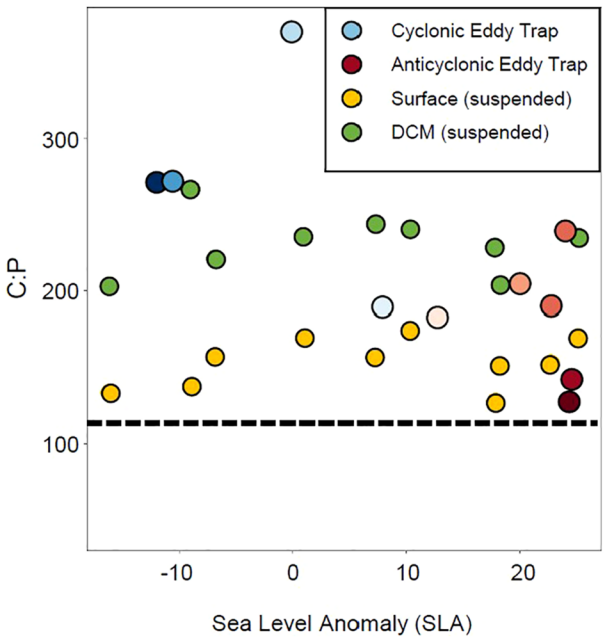

FIGURE 7
The C:P molar ratio of sediment trap lipidomes with water column lipidomes from the surface and DCM across the transect provided for context (full C:P of the water column across the transect found in Supplementary Figure 7). Sea-level anomaly is at the time of deployment for all sediment traps; blue to red shading corresponds to the colors for each trap shown in Figure 6. The dotted line represents the Redfield value for C:P of 106:1.

alleviated stress in the area of increased P, with higher stress signals in areas of depleted phosphorus. Organisms which are highly adapted to the background conditions of the oligotrophic gyre, such as *Prochlorococcus* (Biller et al., 2015), may not benefit from increased fluxes of phosphorus because they are most competitive when nutrients are scarce. Throughout the surface of the transect, dissolved N:P values remained below 10, indicating that nitrogen is the primary limiting nutrient, as is typical for the NPSG (Duhamel et al., 2014; Alexander et al., 2020). We also examined the presence of TAGs as a marker for eukaryotic nutrient stress, as previous studies in algae such as *Chlamydomonas* have shown that these molecules accumulate within cells in response to nutrient starvation (Merchant et al., 2012; Goncalves et al., 2016). Specifically, in *Chlamydomonas*, TAGs increase the most under nitrogen starvation. We found that the TAG: Picoeuk ratio was not correlated to nitrogen concentrations, but instead to SRP, suggesting that TAG overproduction cannot be generalized as a nitrogen stress signal in all contexts. Despite low N:P ratios which indicate N-stress, we still can detect signals of phosphorus quota compensation mechanisms. This suggests that communities still exhibit phosphorus stress physiological responses and therefore may be experiencing varying degrees of co-stress for N and P or a response to low P irrespective of N concentrations. While the observed differences in nutrient concentrations between the eddies are substantial for Station ALOHA, they are relatively small in the context of global variations, highlighting the potential use of lipidomics to yield insight into both fine structure and subtle variations in function within the ecosystem driven by changes in nutrient concentrations and availability.

Exported lipidomes suggest differential cycling within the water column

We can also observe the fate of these stress indicator lipids in sinking particulate organic matter between eddies. The lipids involved in the substitution for P-lipids in cells (i.e., SQDG and the betaine lipids, DGCC, DGTS, and DGTA) have much lower abundance in sediment trap samples than throughout the overlying water column. TAGs, which we suggest are associated with P-stress in this study, have high relative abundances among sinking lipids. PC, a membrane lipid, has a low relative abundance within the water column but is prevalent within the traps—comprising up to a quarter of the lipidome in sinking particulate matter. Our results suggest that lipids used for different physiological functions have different roles in contributing to particulate organic carbon export out of the surface ocean—in particular, that stress-adaptive lipids may be relatively less important in carbon export than other membrane lipids and energy storage lipids.

We further quantified the export rates of lipid classes to identify lipids that are more or less efficiently exported. SQDG, the betaine lipids, and the chlorophylls are exported at low rates. SQDG and divinyl chlorophyll are likely derived primarily from *Prochlorococcus* (Goericke and Repeta, 1992; Popendorf et al., 2011), and the underrepresentation of these lipids relative to the water column in sinking particles is consistent with these organisms making a comparatively small contribution to the sinking flux (Guidi et al., 2016). The BLs, which are primarily derived from eukaryotes and are associated with nutrient stress in these organisms, are also inefficiently exported. We hypothesize that biomass from organisms experiencing nutrient stress and utilizing betaine lipids for growth is either subject to more intense remineralization or sink more slowly. Previous findings have shown that the NPSG in general, and Station ALOHA in particular, is a two-layered system (Karl et al., 2021), with the surface ocean supporting significant primary production, but leading to little export (i.e., intense remineralization of existing resources) (Small et al., 1987). Our finding that betaine lipids are prevalent primarily within the surface ocean but are inefficiently exported supports this framework of a two-layered system. In contrast, the other two lipid molecules primarily derived from eukaryotic microbes (PC and TAGs) are very rapidly exported from the water column.

We observed high rates of export for PC throughout the study, regardless of eddy polarity, suggesting that this observation is not driven by changes in phosphorus concentrations across the transect. We hypothesize that the increased amounts of PC in the traps across the transect may stem from the export of fecal pellets. Findings from single-cell lipidomic work show that PC is enriched in fecal pellets when compared to marine snow aggregates (Hunter et al., 2021). Thus, it is possible that the large PC signal is at least partially due to an increased flux in PC from zooplankton fecal pellets.

In contrast to the elevated signal of PC in the sediments traps, it is less likely that the increased export of TAGs from the cyclonic eddy was a result of zooplankton fecal pellet production. TAGs are generally more enriched in marine snow when compared to fecal pellets (Hunter et al., 2021), and they are generally associated with fresh POM sourced from phytoplankton (Wakeham et al., 1984; Goutx et al., 2003). The strong relationship between the flux of TAGs and ballast minerals suggests that ballast plays a significant role in determining the export of TAGs. We can use differences in lipidomic compositions among eddies to discriminate between mechanisms of sinking particulate organic matter origination and ontogeny. Our study can help us understand what drives the differences in more efficient versus less efficient particulate organic matter export in terms of nutrient perturbations.

Cyclonic eddy perturbation as a mechanism for energy-rich organic material export

If TAG export is driven by mineral ballast, then our data suggest a connection between biomineralization and ocean stoichiometry. High abundances of TAGs greatly increase the C:P ratio of the lipidome of sinking particles compared to suspended particles. Furthermore, the C:P ratio of the lipidome of sinking particles more closely resembles the C:P ratio of suspended particles and lipidomes in the DCM, rather than those observed in the upper euphotic zone. Thus, the C:P ratio of the lipidome is consistent with a significant portion of the exported POM (and mineral ballast) to

originate from the DCM of the water column. This observation lends further evidence for the NPSG as a two-layered system, with a significant portion of export stemming from below the mixed layer (Karl et al., 2021), although this may change with season. These samples were collected during the highly stratified summer months, and equivalent samples do not exist for other seasons. The changes in the C:P ratio of the lipidome of sinking particulate matter have potential implications on the ultimate fate of POM as it travels through the water column. In particular, TAGs represent a store of readily available organic matter and energy (Goutx et al., 2003). The export of TAGs was strongly correlated with the export of both PIC and PSi, two ballast minerals. The increased amount of minerals associated with this exported POM may impact remineralization rates, both because of protection against degradation and due to faster sinking rates (Hedges et al., 2001; Armstrong et al., 2002; Iversen and Ploug, 2010). Indeed, fast sinking speeds and the protection of particles that contain such energy-rich molecules could contribute to enigmatic results observed by Grabowski et al. (2019), where particulate organic matter had high specific energy at abyssal depths, but did not in the mesopelagic. They suggest a model where rapidly sinking particles from the euphotic zone escape most degradation and transformation processes while sinking. Cyclonic eddies commonly harbor increased eukaryotic phytoplankton growth (Landry et al., 2008; Cotti-Rausch et al., 2016), and it is possible that the observed increase in export in the MESO-SCOPE cyclone was due to the presence of larger, denser cells (Armstrong et al., 2002; Klaas and Archer, 2002). Specifically, as shown by Barone et al. (2022), the cyclonic eddy observed during this study contained larger eukaryotes, including those that use minerals important in ballast, such as $CaCO_3$ of coccolithophorids and SiO_2 of diatoms. The potential for ballast-mediated export of TAGs from the cyclonic eddy suggests a role for mesoscale eddy perturbations to contribute to the summer export pulse that is often, but not always, observed at Station ALOHA (Karl et al., 2012).

The study of lipidomes within two eddies in the NPSG reveals changes in both community structure and community behavior in response to changing bottom-up controls, specifically to nutrient concentrations. These changes subsequently impacted the lipidomes of exported material and may have the potential to impact remineralization and sequestration in the deep ocean, via the delivery of energy-rich molecules such as TAGs. While the bulk flux of POC was similar between eddies (Barone et al., 2022), this study demonstrates a potential mechanism for cyclonic mesoscale perturbations to increase the export efficiency of labile particulate organic matter below the euphotic zone.

Data availability statement

The datasets presented in this study can be found in online repositories. The names of the repository/repositories and accession number(s) can be found below: https://zenodo.org/doi/10.5281/zenodo.6390283, hholm/OceanLipidome: Version 1.0.2.

Author contributions

SB: Formal analysis, Writing – original draft, Writing – review & editing. DM: Formal analysis, Writing – review & editing. KB: Conceptualization, Data curation, Formal analysis, Writing – review & editing. BB: Conceptualization, Data curation, Writing – review & editing. TC: Conceptualization, Data curation, Writing – review & editing. HF: Formal analysis, Writing – review & editing. HH: Formal analysis, Writing – review & editing. DK: Conceptualization, Funding acquisition, Writing – review & editing. BV: Conceptualization, Formal analysis, Funding acquisition, Supervision, Writing – original draft, Writing – review & editing.

Funding

The author(s) declare financial support was received for the research, authorship, and/or publication of this article. This work was supported by grants from the Simons Foundation (721229 to BV, 721252 to DK). DM was supported by the Omidyar Postdoctoral Fellowship. SB was supported by the National Science Foundation Graduate Research Fellowship under Grant Nos. 1745302 and 2141064.

Acknowledgments

We thank the captain and crew of the R/V *Kilo Moana* for their assistance during this expedition. We also thank Fiona Hopewell, Tim Burrell, Ryan Tabata, Brandon Brenes, Eric Shimabukuro, and Eric Grabowski for their help with the sample collection. We thank Marissa Small and Kelsey Perry, who were instrumental in sample preparation. The authors also thank Max Jahns and Daniel Lowenstein for their valuable insight during analysis and writing.

Conflict of interest

The authors declare that the research was conducted in the absence of any commercial or financial relationships that could be construed as a potential conflict of interest.

Publisher's note

Author disclaimer

Any opinions, findings, and conclusions or recommendations expressed in this material are those of the authors and do not necessarily reflect the views of the National Science Foundation.

Supplementary material

The Supplementary Material for this article can be found online at: https://www.frontiersin.org/articles/10.3389/fmars.2024.1427524/full#supplementary-material

References

Alexander, H., Rouco, M., Haley, S. T., and Dyhrman, S. T. (2020). Transcriptional response of Emiliania huxleyi under changing nutrient environments in the North Pacific Subtropical Gyre. *Environ. Microbiol.* 22, 1847–1860. doi: 10.1111/1462-2920.14942

Armstrong, R. A., Lee, C., Hedges, J. I., Honjo, S., and Wakeham, S. G. (2002). A new, mechanistic model for organic carbon fluxes in the ocean based on the quantitative association of POC with ballast minerals. *Deep-Sea Res. Part II: Topical Stud. Oceanogr.* 49, 219–236. doi: 10.1016/S0967-0645(01)00101-1

Barone, B., Church, M. J., Dugenne, M., Hawco, N. J., Jahn, O., White, A. E., et al. (2022). Biogeochemical dynamics in adjacent mesoscale eddies of opposite polarities. *Global Biogeochemical Cycles* 36. doi: 10.1029/2021GB007115

Barone, B., Coenen, A. R., Beckett, S. J., McGillicuddy, D. J., Weitz, J. S., and Karl, D. M. (2019). The ecological and biogeochemical state of the North Pacific Subtropical Gyre is linked to sea surface height. *J. Mar. Res.* 77, 509–539. doi: 10.1357/002224019828474241

Becker, K. W., Collins, J. R., Durham, B. P., Groussman, R. D., White, A. E., Fredricks, H. F., et al. (2018). Daily changes in phytoplankton lipidomes reveal mechanisms of energy storage in the open ocean. *Nat. Commun.* 9, 5179. doi: 10.1038/s41467-018-07346-z

Bertilsson, S., Berglund, O., Karl, D. M., and Chisholm, S. W. (2003). Elemental composition of marine Prochlorococcus and Synechococcus: Implications for the ecological stoichiometry of the sea. *Limnol. Oceanogr.* 48, 1721–1731. doi: 10.4319/lo.2003.48.5.1721

Biller, S. J., Berube, P. M., Lindell, D., and Chisholm, S. W. (2015). Prochlorococcus: the structure and function of collective diversity. *Nat. Rev. Microbiol.* 13, 13–27. doi: 10.1038/nrmicro3378

Bligh, E. G., and Dyer, W. J. (1959). A rapid method of total lipid extraction and purification. *Can. J. Biochem. Physiol.* 37, 912–917. doi: 10.1139/y59-099

Chelton, D. B., Schlax, M. G., and Samelson, R. M. (2011). Global observations of nonlinear mesoscale eddies. *Prog. Oceanogr.* 91, 167–216. doi: 10.1016/j.pocean.2011.01.002

Collins, J. R., Edwards, B. R., Fredricks, H. F., and Van Mooy, B. A. S. (2016). LOBSTAHS: An adduct-based lipidomics strategy for discovery and identification of oxidative stress biomarkers. *Analytical Chem.* 88, 7154–7162. doi: 10.1021/acs.analchem.6b01260

Cotti-Rausch, B. E., Lomas, M. W., Lachenmyer, E. M., Goldman, E. A., Bell, D. W., Goldberg, S. R., et al. (2016). Mesoscale and sub-mesoscale variability in phytoplankton community composition in the Sargasso Sea. *Deep-Sea Res. Part I: Oceanographic Res. Papers* 110, 106–122. doi: 10.1016/j.dsr.2015.11.008

Duhamel, S., Björkman, K., Doggett, J., and Karl, D. (2014). Microbial response to enhanced phosphorus cycling in the North Pacific Subtropical Gyre. *Mar. Ecol. Prog. Ser.* 504, 43–58. doi: 10.3354/meps10757

Falkowski, P. G., Ziemann, D., Kolber, Z., and Bienfang, P. K. (1991). Role of eddy pumping in enhancing primary production in the ocean. *Nature* 352, 55–58. doi: 10.1038/352055a0

Foreman, R. K., Segura-Noguera, M., and Karl, D. M. (2016). Validation of Ti(III) as a reducing agent in the chemiluminescent determination of nitrate and nitrite in seawater. *Mar. Chem.* 186, 83–89. doi: 10.1016/j.marchem.2016.08.003

Goericke, R., and Repeta, D. J. (1992). The pigments of Prochlorococcus marinus: The presence of divinylchlorophyll a and b in a marine procaryote. *Limnol. Oceanogr.* 37, 425–433. doi: 10.4319/lo.1992.37.2.0425

Goncalves, E. C., Wilkie, A. C., Kirst, M., and Rathinasabapathi, B. (2016). Metabolic regulation of triacylglycerol accumulation in the green algae: identification of potential targets for engineering to improve oil yield. *Plant Biotechnol. J.* 14, 1649–1660. doi: 10.1111/pbi.12523

Goutx, M., Guigue, C., and Striby, L. (2003). Triacylglycerol biodegradation experiment in marine environmental conditions: definition of a new lipolysis index. *Organic Geochemistry* 34, 1465–1473. doi: 10.1016/S0146-6380(03)00119-0

Grabowski, E., Letelier, R. M., Laws, E. A., and Karl, D. M. (2019). Coupling carbon and energy fluxes in the North Pacific Subtropical Gyre. *Nat. Commun.* 10, 1895. doi: 10.1038/s41467-019-09772-z

Guidi, L., Chaffron, S., Bittner, L., Eveillard, D., Larhlimi, A., Roux, S., et al. (2016). Plankton networks driving carbon export in the oligotrophic ocean. *Nature* 532, 465–470. doi: 10.1038/nature16942

Hedges, J. I., Baldock, J. A., Gélinas, Y., Lee, C., Peterson, M., and Wakeham, S. G. (2001). Evidence for non-selective preservation of organic matter in sinking marine particles. *Nature* 409, 801–804. doi: 10.1038/35057247

Hixson, S. M., and Arts, M. T. (2016). Climate warming is predicted to reduce omega-3 long-chain polyunsaturated fatty acid production in phytoplankton. *Global Change Biol.* 22, 2744–2755. doi: 10.1111/gcb.13295

Holm, H. C., Fredricks, H. F., Bent, S. M., Lowenstein, D. P., Ossolinski, J. E., Becker, K. W., et al. (2022). Global ocean lipidomes show a universal relationship between temperature and lipid unsaturation. *Science* 376, 1487–1491. doi: 10.1126/science.abn7455

Hunter, J. E., Fredricks, H. F., Behrendt, L., Alcolombri, U., Bent, S. M., Stocker, R., et al. (2021). Using high-sensitivity lipidomics to assess microscale heterogeneity in oceanic sinking particles and single phytoplankton cells. *Environ. Sci. Technol.* 55, 15456–15465. doi: 10.1021/acs.est.1c02836

Iversen, M. H., and Ploug, H. (2010). Ballast minerals and the sinking carbon flux in the ocean: carbon-specific respiration rates and sinking velocities of macroscopic organic aggregates (marine snow). *Biogeosci. Discussions*. 7, 3335–3364. doi: 10.5194/bgd-7-3335-2010

Karl, D. M., Church, M. J., Dore, J. E., Letelier, R. M., and Mahaffey, C. (2012). Predictable and efficient carbon sequestration in the North Pacific Ocean supported by symbiotic nitrogen fixation. *Proc. Natl. Acad. Sci.* 109, 1842–1849. doi: 10.1073/pnas.1120312109

Karl, D. M., Letelier, R. M., Bidigare, R. R., Björkman, K. M., Church, M. J., Dore, J. E., et al. (2021). Seasonal-to-decadal scale variability in primary production and particulate matter export at Station ALOHA. *Prog. Oceanogr.* 195, 102563. doi: 10.1016/j.pocean.2021.102563

Karl, D. M., and Tien, G. (1992). MAGIC: A sensitive and precise method for measuring dissolved phosphorus in aquatic environments. *Limnol. Oceanogr.* 37, 105–116. doi: 10.4319/lo.1992.37.1.0105

Klaas, C., and Archer, D. E. (2002). Association of sinking organic matter with various types of mineral ballast in the deep sea: Implications for the rain ratio: Ocean carbon-mineral flux association. *Global Biogeochemical Cycles* 16, 63-1-63–14. doi: 10.1029/2001GB001765

Klausmeier, C. A., Litchman, E., Daufresne, T., and Levin, S. A. (2004). Optimal nitrogen-to-phosphorus stoichiometry of phytoplankton. *Nature* 429, 171–174. doi: 10.1038/nature02454

Knauer, G. A., Martin, J. H., and Bruland, K. W. (1979). Fluxes of particulate carbon, nitrogen, and phosphorus in the upper water column of the northeast Pacific. *Deep-Sea Res.* 26A, 98–108. doi: 10.1016/0198-0149(79)90089-X

Koelmel, J. P., Napolitano, M. P., Ulmer, C. Z., Vasiliou, V., Garrett, T. J., Yost, R. A., et al. (2020). Environmental lipidomics: understanding the response of organisms and ecosystems to a changing world. *Metabolomics* 16, 56. doi: 10.1007/s11306-020-01665-3

Kuhl, C., Tautenhahn, R., Böttcher, C., Larson, T. R., and Neumann, S. (2012). CAMERA: An integrated strategy for compound spectra extraction and annotation of liquid chromatography/mass spectrometry data sets. *Analytical Chem.* 84, 283–289. doi: 10.1021/ac202450g

Landry, M. R., Brown, S. L., Rii, Y. M., Selph, K. E., Bidigare, R. R., Yang, E. J., et al. (2008). Depth-stratified phytoplankton dynamics in cyclone opal, a subtropical mesoscale eddy. *Deep-Sea Res. Part II: Topical Stud. Oceanogr.* 55, 1348–1359. doi: 10.1016/j.dsr2.2008.02.001

McGillicuddy, D. J. (2016). Mechanisms of physical-biological-biogeochemical interaction at the oceanic mesoscale. *Annu. Rev. Mar. Sci.* 8, 125–159. doi: 10.1146/annurev-marine-010814-015606

Merchant, S. S., Kropat, J., Liu, B., Shaw, J., and Warakanont, J. (2012). TAG, You're it! Chlamydomonas as a reference organism for understanding algal triacylglycerol accumulation. *Curr. Opin. Biotechnol.* 23, 352–363. doi: 10.1016/j.copbio.2011.12.001

Muratore, D., Boysen, A. K., Harke, M. J., Becker, K. W., Casey, J. R., Coesel, S. N., et al. (2022). Complex marine microbial communities partition metabolism of scarce resources over the diel cycle. *Nat. Ecol. Evol.* 6, 218–229. doi: 10.1038/s41559-021-01606-w

Oksanen, J., Guillaume Blanchet, F., Friendly, M., Kindt, R., Legendre, P., McGlinn, D., et al. (2020). vegan: community ecology package. Available online at: https://CRAN.R-project.org/package=vegan. (accessed [Sept. 27, 2022]).

Parrish, C. C. (2013). Lipids in marine ecosystems. *ISRN Oceanogr.* 2013, 1–16. doi: 10.5402/2013/604045

Popendorf, K. J., Fredricks, H. F., and Van Mooy, B. A. S. (2013). Molecular ion-independent quantification of polar glycerolipid classes in marine plankton using triple quadrupole MS. *Lipids* 48, 185–195. doi: 10.1007/s11745-012-3748-0

Popendorf, K. J., Lomas, M. W., and Van Mooy, B. A. S. (2011). Microbial sources of intact polar diacylglycerolipids in the Western North Atlantic Ocean. *Organic Geochemistry* 42, 803–811. doi: 10.1016/j.orggeochem.2011.05.003

R Core Team. (2023). R: A language and environment for statistical computing. Available online at: https://www.R-project.org/. (accessed [Sept. 17, 2022]).

Schlitzer, R. (2022). Ocean data viewer. Available online at: https://odv.awi.de. (accessed [Sept. 22, 2022]).

Seki, M. P., Polovina, J. J., Brainard, R. E., Bidigare, R. R., Leonard, C. L., and Foley, D. G. (2001). Biological enhancement at cyclonic eddies tracked with GOES Thermal Imagery in Hawaiian waters. *Geophysical Res. Lett.* 28, 1583–1586. doi: 10.1029/2000GL012439

Signorell, A. (2021). DescTools: Tools for descriptive statistics. Available online at: https://cran.r-project.org/package=DescTools.

Singh, A., Gandhi, N., Ramesh, R., and Prakash, S. (2015). Role of cyclonic eddy in enhancing primary and new production in the Bay of Bengal. *J. Sea Res.* 97, 5–13. doi: 10.1016/j.seares.2014.12.002

Small, L. F., Knauer, G. A., and Tuel, M. D. (1987). The role of sinking fecal pellets in stratified euphotic zones. *Deep-Sea Res.* 34, 1705–1712. doi: 10.1016/0198-0149(87)90019-7

Smith, C. A., Want, E. J., O'Maille, G., Abagyan, R., and Siuzdak, G. (2006). XCMS: processing mass spectrometry data for metabolite profiling using nonlinear peak alignment, matching, and identification. *Analytical Chem.* 78, 779–787. doi: 10.1021/ac051437y

Sweeney, E. N., McGillicuddy, D. J., and Buesseler, K. O. (2003). Biogeochemical impacts due to mesoscale eddy activity in the Sargasso Sea as measured at the Bermuda Atlantic Time-series Study (BATS). *Deep-Sea Res. Part II: Topical Stud. Oceanogr.* 50, 3017–3039. doi: 10.1016/j.dsr2.2003.07.008

Van Mooy, B. A. S., Fredricks, H. F., Pedler, B. E., Dyhrman, S. T., Karl, D. M., Koblížek, M., et al. (2009). Phytoplankton in the ocean use non-phosphorus lipids in response to phosphorus scarcity. *Nature* 458, 69–72. doi: 10.1038/nature07659

Van Mooy, B. A. S., Rocap, G., Fredricks, H. F., Evans, C. T., and Devol, A. H. (2006). Sulfolipids dramatically decrease phosphorus demand by picocyanobacteria in oligotrophic marine environments. *Proc. Natl. Acad. Sci. United States America* 103, 8607–8612. doi: 10.1073/pnas.0600540103

Wacker, A., Piepho, M., Harwood, J. L., GusChina, I. A., and Arts, M. T. (2016). Light-induced changes in fatty acid profiles of specific lipid classes in several freshwater phytoplankton species. *Front. Plant Sci.* 7. doi: 10.3389/fpls.2016.00264

Wakeham, S. G., Lee, C., Farrington, J. W., and Gagosian, R. B. (1984). Biogeochemistry of particulate organic matter in the oceans: results from sediment trap experiments. *Deep-Sea Res. Part A. Oceanographic Res. Papers* 31, 509–528. doi: 10.1016/0198-0149(84)90099-2